Photochemical & Photobiological Sciences

Accepted Manuscript

This is an *Accepted Manuscript*, which has been through the Royal Society of Chemistry peer review process and has been accepted for publication.

Accepted Manuscripts are published online shortly after acceptance, before technical editing, formatting and proof reading. Using this free service, authors can make their results available to the community, in citable form, before we publish the edited article. We will replace this *Accepted Manuscript* with the edited and formatted *Advance Article* as soon as it is available.

You can find more information about *Accepted Manuscripts* in the Information for Authors.

Please note that technical editing may introduce minor changes to the text and/or graphics, which may alter content. The journal's standard Terms & Conditions and the Ethical guidelines still apply. In no event shall the Royal Society of Chemistry be held responsible for any errors or omissions in this *Accepted Manuscript* or any consequences arising from the use of any information it contains.

ROYAL SOCIETY OF CHEMISTRY

www.rsc.org/pps

Location and Freedom of Single and Double Guest in Dye-Doped Polymer Nanoparticles

Cristina Martín, Maria Rosaria di Nunzio, Boiko Cohen, and Abderrazzak Douhal*

Departamento de Química Física, Facultad de Ciencias Ambientales y Bioquímica, and INAMOL, Universidad de Castilla-La Mancha, Avenida Carlos III, S/N, 45071 Toledo, Spain.

*corresponding author: Abderrazzak.Douhal@uclm.es

Phone number: +34-925-265717

Abstract

We report on time-resolved fluorescence anisotropy studies of poly(9-vinylcarbazole) (PVK) nanoparticles (NPs) encapsulating Coumarin 153 (C153) and Nile Red (NR). The wobbling-in-a-cone model successfully describes the restricted movements of the encapsulated molecules. For C153-doped PVK NPs, when increasing the C153 content, the diffusional relaxation (τ_D) times becomes shorter (τ_D = 4.6-1.6 ns) when increasing the C153 content, following its increased preference for less rigid environments. On the other hand, for NR, τ_D is affected by the dopant content (τ_D = 12.2 - 3.09 ns), thus suggesting more rigid environment, which is in agreement with its higher ability to interact with the polymer chains. For the simultaneously two-dye-doped PVK NPs and for the used dye content the orientational dynamics of the trapped guest kept at a fixed content while varying the concentration of the other one slows down (NR; τ_R = 0.30 - 0.37 ns and τ_D = 3.09 - 7 ns) or accelerates (C153: τ_R = 0.14 - 0.03 ns and τ_D = 1.57 - 0.69 ns). This suggests that the guest molecules assume different positions, with C153 preferentially the less rigid environment closer to the NP surface, while NR is located in the more rigid ones, closer to the core. We suggest that the dye distribution within PVK NPs' is governed by the combination of the Marangoni effect, and the consecutive particle swelling. Furthermore, in the two-dye-doped systems, a competition for the available less rigid sites is observed upon increase in the C153 co-dopant content, while in the case of NR as the variable co-dopant this effect is smaller. These findings are relevant to improve on knowledge for a better design of nanophotonic devices based on dye-doped polymer NPs.

Keywords: Wobbling-in-a-cone, Nile Red, Coumarin 153, Poly(9-vinylcarbazole), Hydrophobic, Hydrophilic, Rotational dynamics.

1. Introduction

Over the last twenty years, semiconducting polymers have drawn a growing interest due to their use in light emitting diodes,[1] photovoltaic devices,[2] and as chemical sensors[3] based on the combination of their electronic, optical, and mechanical properties.[4] These properties are sensitive to the mode of preparation of the polymer films and the conditions used, such as solvent, polymer concentration, spin casting speed and treatment after deposition.[5, 6] Therefore, acquiring detailed knowledge on the morphology of the polymer film will allow a better control of the optoelectronic properties of these systems. The parameters involved in the polymers' preparation have been controlled aiming to get insights into the π-π stacking conformation and interactions of the polymeric chains, and their influence on the electronic properties.[4, 7] Nanoparticles (NPs) derived from these polymers have emerged as an attractive solution for controlling the morphology and hence the properties of semiconducting polymer based materials.[8-10]

During the NPs' formation, the hydrophobic polymer chains are sequestered from the polar solvent (water) together with an organic solvent (e.g., tetrahydrofuran, THF) to reach the phase separation. As soon as the polymer has diffused into the "poor" solvent (a solvent where the polymer is less soluble), the polymer chains form the NPs which precipitate or disperse into the solution mixture. This process allows for small hydrophobic fluorescent dyes to be incorporated into the polymer NPs' interior.[11] The possibility to produce dye-doped polymer NPs provides the ability to obtain materials with tunable emission over a wide spectral range,[12, 13] which makes these systems attractive for applications in photonics and bio-imaging.

The nanoprecipitation process to form these polymeric NPs results in the appearance of domains with different characteristics (polarity, hydrophobicity and H-bonding for example) that are localized both in the NPs core and close to its surface. It has been suggested that the Marangoni effect controls the dye distribution within the polymer NPs The Marangoni (also called Gibbs-Marangoni) effect[14] is a physical process comprising a complex interfacial phenomenon of flow, diffusion and surface tension variations. In principal, this flow controls the specific or non-specific interactions between the polymeric units, the dyes and the surface free energy of the dye within the NP. The internal structure of the polymer NPs can be modified by appropriately choosing the polymer-dye mass ratio or the solvents. The formed entity

plays a critical role in its optic and electronic properties and consequently in the performance of the resulting photonic device. Understanding the relationship between the doped polymer NPs characteristics (their nature and relative concentration of doping dyes and the way used to prepare them) with the observed photophysics, will help to optimize the electro-optical properties to those values most adequate for their applications.[15] Several works have studied the energy transfer (ET) processes from excited chromophores of the NPs host to encapsulated dyes.[8, 16] Recently we have demonstrated the multistep cascade ET between the excited cromophores of the polyvinylcarbazole (PVK) NPs host and two trapped dyes (Coumarin 153, C153, and Nile Red, NR), and we have found that its efficiency strongly depends on the dye concentration.[17]

The measurement of the change in polarization of the emitted light gives us the angular rotation of the doping dyes, which is directly correlated to the molecular dynamics near the interaction site.[18] The fluorescence depolarization is a powerful technique to characterize heterogeneous distributions, and hence the local environment of the trapped dyes inside the NPs. It allows us to investigate the tumbling or rotational motion of the guest molecules.[19] It is well known that the increased microscopic friction experienced by a dye within a hosting system (for example, micelles,[20, 21] cyclodextrins,[22, 23] or liposomes[24, 25]) with respect to the bulk conditions, generally leads to slower molecular rotational dynamics. A recent study has reported on an anisotropy measurement of the PVK NPs:NR system and the effect of the varying concentration of the dye.[26] However, information and clear understanding of single and multi-dye distribution within the polymeric NPs and the consecutive specific and nonspecific interactions within the formed domains is still lacking.

Here, we report on time-resolved fluorescence anisotropy studies of PVK NPs encapsulating C153 (PVK:C153), NR (PVK:NR), and both dyes simultaneously (PVK:C153:NR). We analyzed the anisotropy emission decays by means of the wobbling-in-a-cone (WIC) rotational motion model of a dye within a host.[27, 28] This model gives the order parameter related to the restricted movement of the probe, as well as the diffusion coefficients for both, its 'wobbling' and translational motions.[27, 28] The obtained results show a concentration-dependent behavior of the rotational dynamics for single-dye-doped and two-dye-doped PVK NPs systems. Therefore, by knowing the diffusion and rotational times of the guests, as well as their degree of freedom within the host, the analysis provides insights into their distribution and local rigidity.

2. Materials and Methods

All the chemicals were purchased from Sigma-Aldrich. Poly(9-vinylcarbazole) (PVK, average M_W ~ 35000), Coumarin 153 (C153, 99%), Nile Red (NR, 99%), and tetrahydrofuran (THF, spectroscopic grade >99.5 %) were used as received. The preparation and characterization methods of the doped PVK NPs were described elsewhere.[17] A simple re-precipitation method has been applied to prepare the dye doped PVK polymer nanoparticles. The THF was then partially removed using vacuum evaporation of the obtained suspensions. After the NPs formation, the suspensions were filtered using a 0.2 micron filter to remove PVK aggregates in the microscale region.[17] Pure PVK and doped PVK monodispersed NPs in aqueous suspensions are obtained. To ensure that all the dye molecules were embedded inside the NPs we checked the optical density (absorption and emission spectra) before and after dialysis using a dialysis membrane molecular cut-off of 12-14 kDa.[17] The comparison between the emission spectra of the different dye-encapsulated PVK NPs before and after 0.2-micron membrane filtration suggests that, the preparation yield of the dye-doped NPs is above 90% in each case. This also suggests that almost 90% of the PVK polymer chains are converted into (< 100 nm) NPs.[17] For these systems it has been shown that the PVK NPs present a diameter between 50-70 nm. It is important to note that the average size of the polymer NPs remains unaltered even in presence of the highest doping of C153 and NR (2.72 % wt of C153 and 1.6 % wt of NR in PVK:C153:NR).[17] Three days following the NPs preparation, the measured optical density of the initial suspension showed that almost 98% of the dye molecules were still encapsulated, indicating a non-significant dye leakage within that period.[17]

Picosecond (ps) time-resolved emission measurements were carried out using a time-correlated single-photon-counting (TCSPC) spectrophotometer (Fluotime 200, PicoQuant) previously described. The sample was excited with a femtosecond (fs) pulse form a Ti:sapphire oscillator (Mai Tai HP, Spectra Physics) coupled to a second harmonic generator. The pulses (100 fs, 40 MHz, 1 mW) were centered at selected wavelengths (410, and 510 nm) and the emission wavelength was collected at the magic angle (54.7º). The instrument response function (IRF) was typically from 30-60 ps depending on the excitation wavelength. The time-resolved ps anisotropy was constructed using the expression $r(t) = (I_{||}-GI_{\perp})/(I_{||}+2GI_{\perp})$, where G is the ratio between

the fluorescence intensity at parallel ($I_{\parallel}$) and perpendicular ($I_{\perp}$) polarizations of the emission with respect to the excitation beam. The value of G was measured at a gating window, in which the fluorescence is almost completely depolarized (tail-matching technique). The anisotropy decay curves were deconvoluted to the IRF and fitted to a multi-exponential function using the Fluofit package (PicoQuant). The quality of the fit was characterized in terms of the residual distribution and reduced χ^2 values.

The following function was used to extract the WIC parameters:

$$r(t) = r_0[S^2 + (1 - S^2)\exp(-t/\tau_R)]\exp(-t/\tau_D)] \quad (1)$$

with $S = 0.5\cos\theta_0\ (1 + \cos\theta_0)$, where r_0 is the anisotropy at t = 0, S is the order parameter (equal to 0 for completely free motion and 1 for the completely restricted one), τ_R and τ_D are the fast wobbling motion and the slow lateral diffusion times of the dye, and θ_0 is the cone (revolution cone defined by the wobbling motion) semi-angle during the wobbling motion. The WIC model has been used to elucidate the orientational dynamics of several dyes within polymer NPs.[26, 29] In our case, NR and C153 are not covalently bonded to the polymer chains, and therefore have some freedom in diffusion and rotational motions inside the PVK NPs. The variability of the obtained data has been calculated and it is indicated in the Figures by an error bar. All the experiments were done at 293 K.

3. Results and Discussion

3.1. Steady-State Observations

Figure 1S in SI shows the UV-visible absorption and emission spectra of the PVK:C153, PVK:NR, and PVK:C153:NR NPs in water suspensions. The absorption spectra show, in addition to the band around 345 nm (due to the PVK chromophore), two relatively weak intensity absorption bands at 420 and 525 nm, corresponding to the dyes (C153 and NR, respectively) inside the PVK NPs. Upon the encapsulation of the dye (2.72 wt% of C153 or 1.60 wt% of NR), the emission of PVK following excitation at 350 nm is partially quenched, while an emission from the trapped C153 or NR is observed. In presence of both dyes within the PVK NPs (2.7 wt% of C153 and 1.60 wt% of NR), the polymer emission is efficiently quenched along with a significant quenching of the C153 emission (at 510 nm). This is a clear indication that the studied systems undergo efficient multistep cascade ET from the 350 nm-excited PVK host to NR through C153, the latter acting as a light harvester.[17]

To exclude the hetero-ET as a possible origin of the emission depolarization,[18] we avoid the 350 nm-excitation (PVK absorption maxima) and excite the systems at the absorption maxima of the dyes (410 nm for C153 and 510 nm for NR). Additionally, when the Stokes shift is small, the ET between identical chromophores (homo-ET) can shorten the anisotropy decay of the system.[30] To get an efficient homo-ET the two chromophores must be in close proximity and a good spectral overlap (J(λ)) of the emission and absorption is needed. For the single chromophore doped systems used here, and for the highest dopant concentrations, we have calculated that the minimum distance required for the homo-ET is 2.18 and 2.84 nm for 2.7 % wt C153 and 1.6 % wt NR doped NP, respectively. Assuming a homogeneous distribution of the chromophore molecules within the NP, the estimated homo-ET efficiencies are 11% and 15%, respectively (see the SI for details about the calculations). On the other hand, at these contents the average distance between the encapsulated molecules within a ~ 60 nm NP is 3.05 and 3.75 nm, for C153 and NR, respectively. These distances, longer (by ~ 1 nm) than the required for the homo-ET, indicate that although we cannot discard entirely the presence of homo-ET, its effect on the anisotropy decay of these systems will be very weak.

Below we present and discuss the obtained results for one-dye and two-dye-doped PVK NPs without taking into account the possible but small contribution of the homo-ET in the anisotropy decay.

3.2. Time-Resolved Picosecond Fluorescence Anisotropy

3.2.1. One-Dye-Doped Nanoparticles

PVK:C153 (0.22 - 2.72 wt%): Figure 1A shows the emission anisotropy decays, r(t), for the aqueous PVK:C153 NPs suspensions at two representative doping degrees (0.22 and 2.72 wt%) of C153. We excited (410 nm) and observed (510 nm) an ensemble of trapped C153 within PVK NPs.

We have found that a bi-exponential function well reproduces the anisotropy decays in the whole investigated range of the used guest contents (0.22 - 2.72 wt%). The data are shown in Table 1SA in SI. The rotational times at the lowest used C153-doping (0.22 wt%) are ϕ_1 = 190 ps and ϕ_2 = 4.63 ns, corresponding to the reorientation times associated with the fast (τ_{fast}) and slow (τ_{slow}) motions of C153 within the PVK NPs, respectively. The decrease of r_0 value (from 0.38 in water[31] to 0.12 for PVK:C153 at 0.22 wt% C153-doping) suggests a very fast depolarization (below our time

resolution, ~ 20 ps) of the C153 emission inside the PVK NPs with respect to its free form. This agrees with previous studies, where r_0 for C153 is reported to generally decrease in heterogeneous media.[32-36] When the C153 content increases up to 2.72 wt%, the rotational times become shorter going from 190 to 130 ps and from 4.6 to 1.6 ns for ϕ_1 and ϕ_2, respectively (Table 1SA in SI). In contrast, the r_0 value (0.19) does not show significant change. As the results indicate, the dye content clearly affects the rotational dynamics of the encapsulated C153 molecules.

Analyzing the anisotropy decays by means of the WIC model (see SI for details), we found that when the C153-doping increases, both the fast wobbling rotational (τ_R) and slow lateral diffusion (τ_D) times monotonically decrease by 30% (from 0.20 to 0.14 ns) and 66% (from 4.6 to 1.6 ns) for τ_R and τ_D, respectively. It should be noted that, due to the large difference in the experimental values of ϕ_1 and ϕ_2, on one hand, and τ_M (overall rotation of the polymer NP), on the other hand, the values of τ_R and τ_D obtained from the WIC model (see SI) are comparable (almost identical) to τ_{fast} and τ_{slow}, respectively. They display different dependence on dye content: linear for τ_R and exponential for τ_D (Figure 3A). Although both τ_D and τ_R decrease with the increase of C153 concentration, the value of τ_D is affected more strongly than that of τ_R. This difference can be explained by the different free volumes around the encapsulated guest molecules that are required for the wobbling and the translation motions within the PVK NP. However, the general behavior of both τ_D and τ_R suggests an increased freedom for both motions upon increasing C153 concentration, which in turn indicates that the molecule moves from more restrictive to less restrictive environment. Similar behaviour has been previously reported for the fluorescence anisotropy decays of two dyes (merocyanine 540 and oxazine 1) in a polymer-surfactant aggregate containing poly(vinylpyrrolidone) (PVP) and sodium dodecyl sulphate (SDS).[37] This change in the characteristics of the local environment around the encapsulated C153 is further reflected by the square order parameter (S^2) and the cone semi-angle (θ_0) values (Figure 3B and Table 1). Both S^2 and θ_0 reflect the internal motion of trapped C153 molecules wobbling inside a cone and they undergo, respectively, a ~ 0.5-fold decrease (from 0.62 to 0.33) and a 1.5-fold increase (from 32º to 47º), as the C153 content goes from 0.22 to 2.72 wt%. Lower values for the order parameter (and higher ones for the cone semi-angle) indicate that the embedded dye molecules are experiencing less restricted rotation within the polymer NP. The anisotropy decay parameters allow us to estimate

the diffusion coefficients for wobbling (D_W) and translational diffusion (D_L) motions by using Equations 7 -14 in SI.[27, 28] Table 1 gives the obtained values for the PVK:C153 system. The D_L and D_W values increase with the dye content according to the changes in τ_D, τ_R, S^2 and θ_0 values. The relatively high values of D_W and D_L, as well as their monotonic increase with the C153 concentration are evidence that the dye molecules, at high concentrations, have higher mobilities, which is consistent with higher occupancy of sites closer to the NP surface having less rigid environment.

PVK:NR (0.63 - 1.60 wt%): Figure 1B shows two representative emission anisotropy r(t) decays of the PVK:NR NPs in water suspensions (0.63 and 1.60 wt% of NR). The decays are collected exciting the encapsulated NR at 510 nm and observing at 610 nm, which are the wavelengths of absorption and emission intensity maxima of the dye, respectively. The best fit requires three components (ϕ_1, ϕ_2, and ϕ_3 in Table 1SB in SI) in the whole investigated range of NR contents. The shorter component (ϕ_1 ~ 16 ps, on the limit of the resolution after IRF convolution), not observed in pure water (ϕ = 50 ps),[38] and the low value of r_0 (0.17) suggest a fast depolarization as a result of an intramolecular charge-transfer process.[39] The excited-state dynamics of NR has been described by a two-state model.[39] The locally-excited-state (LE) of NR can be stabilized by solvent reorganization prior to undergoing twisting motion and formation of non-emissive twisted intramolecular charge-transfer (TICT) state.[39] This process has been observed for NR in membranes, micelles, and in highly viscous alcohols.[40, 41] Upon excitation, NR at S_1 undergoes a significant change in its dipole moment ($\Delta\mu$ ~ 11.6 D), which results in the reorganization of the solvent molecules dipoles around its excited-state.[41] This relaxation process is generally of the order of a few tens of ps in pure solvents of low viscosities, while its value increases with the viscosity of the medium or in water contained in organized media.[42] While both ϕ_1 (16 ps) and ϕ_2 (~ 300 ps, τ_{fast} in the WIC model, Table 1SB in SI) do not show significant changes in the studied range of NR contents, the longest time constant (ϕ_3, τ_{slow} in the WIC model) is reduced by ~ 75% of its initial value (from 12.2 to 3.09 ns) when using 0.63 and 1.60 wt% of NR within the PVK NPs, respectively. Comparable results have been observed for NR-encapuslated PVK NPs with a larger diameter (100 nm) using fluorescence anisotropy studies.[26] In particular, it has been observed that, for these systems, the anisotrpy (average rotational times, $\langle\tau_r\rangle$) decreases from 3.57 to 0.545 ns when the NR-doping goes from 0.5 to 1.8 wt%.[26] The authors have explained the results on the basis of an

emission depolarization process, without taking into account the possible influence of the dye distribution/localization on its rotational dynamics inside the PVK NPs' domains.

The results for NR-doped PVK NPs after applying the WIC model are presented in Figures 4A-B and in Table 1. As Figure 4A shows, there is almost no variation of τ_R with the wt% of NR, preserving an average value of 0.31 ns. However, τ_D is clearly affected by the dopant content, decreasing by 75% (from 12.2 to 3.09 ns) in the 0.63-1.60 range of NR wt%. The different behavior can be explained, similarly to the case of C153, by a different sensitivity of these motions to the local environment around the NR molecules during the two relaxation times. The quasi-invariance of τ_R value (~ 0.31 ns) with the dye-doping suggests no significant changes in the interactions between NR and the polymer chains independently on the occupied sites. The order parameter is reduced from 0.67 to 0.52, corresponding to a cone semi-angle variation from 29º to 37º (Table 1). This change indicates a small increase in the internal motion of the trapped molecules with their content, which in turn indicates a less restrictive environment.

The relaxation of NR within the PVK NPs is clearly slower than that of C153 in the same dye-content window (0.5 - 2 wt%, Table 1). More specifically, at dye content of ~ 0.5 wt%, the τ_R and τ_D values of NR are, in that order, ~ 1.6 and ~ 3.6 times longer than those of C153. Although both dyes present comparable volumes (3.69 and 4.19 / 10^{-22} cm^3 for C153 and NR, respectively; calculated by modelling the molecules as an oblate spheroid, non-hydrated rotors)[43, 44], NR has larger a ground state dipole moment (μ_g = 8.2 D)[45] in comparison with that of C153 (μ_g = 6-7 D)[46]. This difference in the μ_g might lead NR to inhabit more polar sites, most probably in proximity with the bulkier aromatic carbazole groups. Due to the presence of these bulky aromatic side groups the packing of the polymer chains within the spherical nanoparticle will be hindered resulting in different local free volumes.[47] The higher restriction for NR motion within the PVK NPs leads, consequently, to higher dependence of τ_D with the dye-doping with respect to C153. In the case of PVK:NR NPs, changes in the value of D_W, (2.2 - 3.56) × 10^8 s^{-1}, are observed in the studied dye content range. This is in agreement with the trends observed for τ_R, S^2, and θ_0. The higher D_W values calculated for C153 in PVK:C153 with respect to those obtained for NR in PVK:NR further support the fact that the C153 and NR molecules in the one-dye-doped system assume different

locations, being less restricted for C153 (closer to the NP surface), while more rigid for NR (closer to the NP core).

The general behavior of both one-dye doped systems is consistent with a random distribution of the encapsulated chromophores suggested for other polymer nanoparticles.[11] However, the values of the parameters obtained from the WIC model indicate additional radial dependence of the distribution with the increase in the dopant concentration.[11] At low dye content it is expected that the majority of the hydrophobic dye molecules will be distributed closer to the more densely packed (and thus more rigid) NP core, with a small percentage found in the vicinity of the nanoparticle surface. Single molecule studies have demonstrated the existence of sites with different free volumes in poly(methyl methacrylate) and poly(*n*-butyl methacrylate) polymer films resulting in different behavior of the probe molecules.[48] Ensemble average studies on the effect of the temperature and alkyl groups of poly(alkyl methacrylate) on inter- and intramolecular interaction of pyrenyl guest molecules have found that the segmental relaxation close to the probe molecules also plays a significant role in its photodynamics.[49] We suggest that in both, the PVK:C153 and the PVK:NR systems, the dye molecules at low concentrations occupy preferentially the sites at the core of the NPs, which are the most rigid ones (Scheme 2). Upon increasing the dopant content, the trapped dye molecules start to distribute in a way (radial-like) that they begin to also occupy less rigid sites with larger free volumes and with less restriction, and which are located close to the NP surface. Besides this, our results suggest that the trapped NR molecules will be located predominantly closer to the core of the NP with stronger rigidity and restriction to lateral and wobbling motion, as observed by the analysis of its orientational dynamics. It should be noted that the reported dependence is based on ensemble average measurements, where we observe the collective behavior of an ensemble of molecules encapsulated within polymer NPs.

3.2.2. Two-Dye-Doped Nanoparticles

PVK:C153:NR: Having characterized the one-dye-doped PVK NPs, we have examined how the co-existence of both C153 and NR as dopant molecules at different molar fractions affects their relative anisotropy behaviour within the polymeric network of the formed nanosystems. We performed experiments with the PVK:C153:NR NPs in water suspensions by varying the initial content of one of the dyes (C153 or NR) while keeping constant the other one (NR or C153, respectively).

Case A (constant NR, variable C153): We first look at the PVK:C153:NR system at the lowest (0.14 wt%) and highest (2.72 wt%) C153-dopings when the NR content is fixed to 1.60 wt%. Figure 2A shows two representative anisotropy decays of the water suspensions exciting at 510 nm and observing at 610 nm, where the absorption and emission are due to trapped NR. We find a three-exponential behavior of r(t) in the studied range of C153 contents (Table 1SC in SI). The ps-component (ϕ_1 = 22 ps) is ascribed, as for the case of the PVK:NR system, to a fast depolarization due to the formation of the TICT state of NR in its excited-state. The time constants ϕ_2 and ϕ_3 are related to the fast (τ_{fast}) and slow (τ_{slow}) motions of trapped NR, respectively. Their values clearly follow an opposite trend with respect to that observed in PVK:NR. Both times, ϕ_2 = 0.27 - 0.37 ns and ϕ_3 = 3.09 - 7.00 ns, increase as the initial content of C153 goes from 0 to 2.72 wt%. The r_0 value, being 0.17 in the absence of C153, grows up to 0.22 at the C153-doping maximum.

Figure 5 exhibits the changes of τ_R, τ_D, S^2, and θ_0 with the guest content, while Table 2 shows the related values obtained by applying the WIC model in the range of the studied wt%. Upon increasing the amount of C153, the orientational dynamics of the NR at fixed content (1.60 % wt) slows down. In particular, we found that while the wobbling time (τ_R) exhibits a very small change, the lateral relaxation time (τ_D) of NR increases (from 3.09 to 7 ns) when the amount of C153 increases from 0 to 2.72 wt% (Figure 5A and Table 2). This change suggests that the added C153 molecules displace the NR ones from regions with less rigidity (closer to the surface) to those of higher rigidity (closer to the NP core) thereby occupying similar sites like at ~ 1 wt % in the single dye-doped system for PVK:NR (Table 1). The effect of the C153 content on the S^2 and θ_0 values for the trapped NR is shown in Figure 5B. We can distinguish three regions:

Region I (C153 wt% < 0.8): At these contents of C153 (C153:NR stoichiometric ratio maximum = 0.5), we observe a sharp decrease (~ 40%) in the S^2 value. The cone semi-angle of NR increases from 37º to 47º. This is explained in terms of occupancy of sites within the PVK NP having lower rigidity. Region II (0.8 ≤ C153 wt% ≤ 1.6): S^2 and θ_0 values tend to either increase or decrease, respectively, until reaching a plateau of ~ 0.40 and 44º at wt% C153 = 1.60 (C153:NR stoichiometric ratio = 1). This inversed trend suggests that NR molecules are displaced to occupy different positions of higher local rigidity at higher C153 contents. Region III (C153 wt% > 1.6): S^2 and θ_0 values

reach a plateau and do not show any variation when the C153 content is higher than 1.6 wt%. This indicates that, at larger C153 contents (C153:NR stoichiometric ratio larger than 1), the sites occupied by NR molecules have similar local rigidities and thus similar volumes. The calculated D_L values for this system change from 4.85 to 2.14 × (10^{-8} m^2 s^{-1}) (Table 2). D_W experiences a small change and it reaches its maximum at 0.54 % wt of C153, when θ_0 and S^2 have their maximum and minimum, respectively.

Case B (constant C153, variable NR): The second PVK:C153:NR system which we have examined is when the content of C153 is fixed at 2.72 wt%, while varying that of NR (from 0 to 1.60 wt%). Figure 2B shows the anisotropy decays at 0.08 and 1.60 wt% of NR. The excitation (410 nm) and emission (510 nm) wavelengths are those of trapped C153. Table 1SD in SI gives the obtained anisotropic parameter values after fitting the decays to bi-exponential functions. As the wt% of NR increases from 0 to 1.60, a clear shortening is observed for both ϕ_1 (τ_{fast} from 0.13 to 0.03 ns) and ϕ_2 (τ_{slow} form 1.57 to 0.69 ns). The r_0 value is 0.19 when the wt% NR = 0, and it reaches 0.38 at the highest used NR-content (1.60 wt%).

The WIC model analysis of this system, demonstrates that increasing the NR content accelerates the orientational dynamics of the fixed C153 (Figure 6A and Table 3). In contrast with the system where the concentration of the C153 is varied, we found that both relaxation times of C153 (fixed at 2.72 wt%) decrease, corresponding to an increase in the rotation and diffusion freedom (Figure 6A and Table 3). The effect of the NR content on the S^2 and θ_0 values for the trapped C153 is shown in Figure 6B. For this system, we find two regions:

Region I, NR wt% ≤ 0.63: The wobbling (τR) and lateral (τD) times, in this case, are shortened by 68% (from 0.14 to 0.045 ns) and 50% (from 1.57 to 0.78 ns) of their initial values, respectively, in the 0 – 0.63 range of NR wt% (Figure 6A and Table 3). This is also reflected by a ~ 0.5-fold reduction (from 0.33 to 0.17) of S2 and a 1.2-fold increase (from 47º to 57º) of θ_0 (Figure 6B). Region II, NR wt% ≥ 0.63: The values of τ_R (~ 0.045 ns), τ_D (~ 0.78 ns), S2 (0.17) and θ_0 (57º) of C153 reach a plateau. With this amount of NR, in this region, the trapped C153 molecules clearly feel less restriction to their motions, and tend to inhabit sites closer to the nanoparticle surface of lower rigidity, contrary to NR molecules preference. The increased mobility of C153 at high NR content is also reflected in the values of D_W and D_L, as both gradually increase with NR concentration (Table 3).

The observed anisotropy behavior of the two-dye-doped PVK NPs can be explained in terms of the dye competition for the free domains at higher dye concentrations. Following the initial nucleation and encapsulation process, the distribution of the guest molecules inside the NPs will be strongly affected by the onset of the Marangoni effect due to the partition equilibrium between the aqueous and the organic phases, the molecule-polymer interactions, and the polymer precipitation rate.[50] The Marangoni effect is explained in terms of a flow which governs the formation of the NPs.[14] In our case, the difference between the surface tension values of THF (26.40 $\times$ 10^{-3} Nm^{-1} at 293 K)[51] and water (72.80 $\times$ 10^{-3} Nm^{-1} at 293 K)[51] is reasonably large to create a surface-tension-gradient-induced motion of THF, by carrying it toward the contact line and into the water phase. At the same time, the dye (NR or C153) dissolved in THF will be dispersed into the polymer particle through this surface tension gradient force. Thus, the initial concentration of the guest, as well as its interactions with the PVK chains, determine its location inside the polymer NP during the surface-tension-gradient-induced dispersion.

Another process that can influence the particle formation, growth and the consecutive dye distribution is the Ostwald ripening.[52] At longer times, the particles can grow more by diffusion of the PVK to PVK NPs forming larger particles from the smaller ones. Such a slow process can increase the polydispersion of the NPs and also reduce the NPs stability. However, removing the organic solvent (THF) from the water suspensions significantly reduces this phenomena.[53] Additionally, once THF has been evaporated, some water molecules can penetrate within the porous structure of the PVK NPs and possibly modify the position of the guest molecules. The migration of water molecules to the interstices of the polymer coils will force them to "swell" following the PVK NPs' formation.[54] This process generally occurs on longer time scales than the Marangoni effect. As a result of the combination of these effects different domains and local environments are formed within the nanostructure.[17] Hence, in the systems under study, the Marangoni effect and the NPs swell can explain the different distributions assumed by the encapsulated dyes (Scheme 2) and the resulting differences in the interactions with the polymer chains following the PVK NPs' formation. The preferential location of C153 at the periphery of the PVK NP at higher contents may cause a "collapse" of the NP core leading to a restriction to host the NR molecules. However, we can not exclude that at much longer times partial equilibration due to NP swelling may occur. This process will be limited by the interactions within the formed

domains. We didn't observe a change in the photobehavior of the system over several days, suggesting a fast equilibrium, in the formed doped NPs.

4. Conclusions

In summary, we have studied the time-resolved emission anisotropy behaviour of PVK NPs containing C153, NR, and both dyes simultaneously. The wobbling-in-a-cone model successfully describes the restricted movements of the encapsulated molecules. For C153-doped and NR-doped PVK NPs, the diffusional (τ_D) relaxation time become shorter (τ_D = 4.6 - 1.6 ns) when increasing the C153 contents. However, for NR, only τ_D is affected by the dopant content (τ_D = 12.2 - 3.09 ns), while τ_R preserves a value of 0.31 ns. The behaviour of the WIC parameters suggests radial distribution (from the core to the surface) of both dyes in the PVK NPs with increasing the dopant concentration. Interestingly, for the simultaneously two-dye-doped PVK NPs: the diffusion times of the trapped guests kept at a fixed content slows down (NR; τ_D = 3.09 - 7 ns) or accelerates (C153; τ_D = 1.57 - 0.69 ns). These results are explained on the basis of different distributions of the dye molecules inside the PVK NPs at the moment of their encapsulation. For the two-dye-doped PVK NPs, we found that the preferential location of C153 within the less rigid environments and that of NR in the more rigid ones lead to different behaviour of the re-orientational times when the second guest content increases. The guest distribution within the NPs is explained in terms of a combination of Marangoni effect and the swell of the NPs and the competition to habit different sites. These findings bring new insight into host-guest interactions of the rotational dynamics of two well known fluorescent dyes in supramolecular systems, and, in particular, should improve our knowledge for a better design of nanophotonic devices based on dye-doped polymer NPs.

Acknowledgements

This work is supported by the bilateral Spanish-Indian cooperation research through MINECO (PRI-PIBIN-2011-1283) and MAT2011-25472. C. M. thanks the MEC for the FPU PhD fellowship, and MRD the CYTEMA contract.

Supporting Information: Detailed information about of the wobbling-in-a-cone model and ET calculation. Normalized UV-visible absorption and emission spectra of water suspensions containing pure and doped-PVK polymer NPs. Values of anisotropic decay parameters (rotational time constants, ϕ_i; normalized (to 100) pre-exponential factors, A_i; fundamental anisotropy, r_0) for the studied doped-PVK polymer NPs. This material is available free of charge via the Internet.

References:

1. R. H. Friend, R. W. Gymer, A. B. Holmes, J. H. Burroughes, R. N. Marks, C. Taliani, D. D. C. Bradley, D. A. Dos Santos, J. L. Brédas, M. Lögdlund and W. R. Salaneck, *Nature*, 1999, **397**, 121-128.
2. T. M. Clarke and J. R. Durrant, *Chem. Rev.*, 2010, **110**, 6736-6767.
3. S. W. Thomas, G. D. Joly and T. M. Swager, *Chem. Rev.*, 2007, **107**, 1339-1386.
4. F. J. M. Hoeben, P. Jonkheijm, E. W. Meijer and A. P. H. J. Schenning, *Chem. Rev.*, 2005, **105**, 1491-1546.
5. B. J. Schwartz, *Annu. Rev. Phys. Chem.*, 2003, **54**, 141-172.
6. J. C. Bolinger, M. C. Traub, J. Brazard, T. Adachi, P. F. Barbara and D. A. Vanden Bout, *Acc. Chem. Res.*, 2012, **45**, 1992-2001.
7. A. Facchetti, *Chem. Mater.*, 2010, **23**, 733-758.
8. Z. Tian, J. Yu, C. Wu, C. Szymanski and J. McNeill, *Nanoscale*, 2010, **2**, 1999-2011.
9. D. Tuncel and H. V. Demir, *Nanoscale*, 2010, **2**, 484-494.
10. J. Pecher and S. Mecking, *Chem. Rev.*, 2010, **110**, 6260-6279.
11. C. Wu, Y. Zheng, C. Szymanski and J. McNeill, *J. Phys. Chem. C*, 2008, **112**, 1772-1781.
12. J. L. West and N. J. Halas, *Annu. Rev. Biomed. Eng.*, 2003, **5**, 285-292.
13. C. Zhong, C. Duan, F. Huang, H. Wu and Y. Cao, *Chem. Mater.*, 2010, **23**, 326-340.
14. L. E. Scriven and C. V. Sternling, *Nature*, 1960, **187**, 186-188.
15. S. Sarzi Sartori, S. De Feyter, J. Hofkens, M. Van der Auweraer, F. De Schryver, K. Brunner and J. W. Hofstraat, *Macromolecules*, 2002, **36**, 500-507.
16. C. Wu, Y. Zheng, C. Szymanski and J. McNeill, *J. Phys. Chem. C*, 2008, **112**, 1772-1781.
17. C. Martin, S. Bhattacharyya, A. Patra and A. Douhal, *Photochem. Photobiol. Sci.*, 2014, 10.1039/c1034pp00086b.
18. J. R. Lakowicz, *Principles of Fluorescence Spectroscopy*, 4th edn., Springer US, 2006.
19. D. M. Jameson and J. A. Ross, *Chem. Rev.*, 2010, **110**, 2685-2708.
20. G. B. Dutt, *J. Phys. Chem. B*, 2008, **112**, 7220-7226.
21. A. Douhal, G. Angulo, M. Gil, J. Á. Organero, M. Sanz and L. Tormo, *J. Phys. Chem. B*, 2007, **111**, 5487-5493.
22. D. Zhong, A. Douhal and A. H. Zewail, *Proc. Natl. Acad. Sci. U.S.A.*, 2000, **97**, 14056-14061.
23. A. Douhal, *Chem. Rev.*, 2004, **104**, 1955-1976.
24. B. K. Paul and N. Guchhait, *J. Colloid Interface Sci.*, 2011, **363**, 529-539.
25. C. R. Mateo and A. Douhal, *Proc. Natl. Acad. Sci. U.S.A.*, 1998, **95**, 7245-7250.
26. S. Bhattacharyya, S. Prashanthi, P. R. Bangal and A. Patra, *J. Phys. Chem. C*, 2013, **117**, 26750-26759.
27. G. Lipari and A. Szabo, *Biophys. J.*, 1980, **30**, 489-506.
28. N. C. Maiti, M. M. G. Krishna, P. J. Britto and N. Periasamy, *J. Phys. Chem. B*, 1997, **101**, 11051-11060.
29. S. Bhattacharyya, B. Paramanik and A. Patra, *J. Phys. Chem. C*, 2011, **115**, 20832-20839.
30. M. N. Berberan-Santos and B. Valeur, *J. Chem. Phys.*, 1991, **95**, 8048-8055.

31. T. J. V. Prazeres, M. Beija, F. V. Fernandes, P. G. A. Marcelino, J. P. S. Farinha and J. M. G. Martinho, *Inorg. Chim. Acta*, 2012, **381**, 181-187.
32. A. Chakraborty, D. Seth, D. Chakrabarty, P. Setua and N. Sarkar, *J. Phys. Chem. A*, 2005, **109**, 11110-11116.
33. D. Seth, A. Chakraborty, P. Setua and N. Sarkar, *J. Phys. Chem. B*, 2007, **111**, 4781-4787.
34. P. Sen, D. Roy, S. K. Mondal, K. Sahu, S. Ghosh and K. Bhattacharyya, *J. Phys. Chem. A*, 2005, **109**, 9716-9722.
35. D. Roy, S. K. Mondal, K. Sahu, S. Ghosh, P. Sen and K. Bhattacharyya, *J. Phys. Chem. A*, 2005, **109**, 7359-7364.
36. D. Chakrabarty, D. Seth, A. Chakraborty and N. Sarkar, *J. Phys. Chem. B*, 2005, **109**, 5753-5758.
37. S. Sen, D. Sukul, P. Dutta and K. Bhattacharyya, *J. Phys. Chem. A*, 2001, **105**, 7495-7500.
38. P. Hazra, D. Chakrabarty, A. Chakraborty and N. Sarkar, *Chem. Phys. Lett.*, 2004, **388**, 150-157.
39. A.-Y. Jee, S. Park, H. Kwon and M. Lee, *Chem. Phys. Lett.*, 2009, **477**, 112-115.
40. P. J. G. Coutinho, E. M. S. Castanheira, M. Céu Rei and M. E. C. D. Real Oliveira, *J. Phys. Chem. B*, 2002, **106**, 12841-12846.
41. M. M. G. Krishna, *J. Phys. Chem. A*, 1999, **103**, 3589-3595.
42. A. Datta, D. Mandal, S. K. Pal and K. Bhattacharyya, *J. Phys. Chem. B*, 1997, **101**, 10221-10225.
43. C. M. Hu and R. Zwanzig, *J. Chem. Phys.*, 1974, **60**, 4354-4357.
44. J. S. Baskin and A. H. Zewail, *J. Phys. Chem. A*, 2001, **105**, 3680-3692.
45. A. Kawski, P. Bojarski and B. Kukliński, *Chem. Phys. Lett.*, 2008, **463**, 410-412.
46. R. Kanya and Y. Ohshima, *Chem. Phys. Lett.*, 2003, **370**, 211-217.
47. J. Duda and J. M. Zielinski, eds., *Free-Volume Theory*, 1996.
48. R. A. L. Vallée, M. Cotlet, M. Van Der Auweraer, J. Hofkens, K. Müllen and F. C. De Schryver, *J. Am. Chem. Soc.*, 2004, **126**, 2296-2297.
49. S. Abraham, T. D. Z. Atvars and R. G. Weiss, *J. Phys. Chem. B*, 2010, **114**, 12221-12233.
50. C. E. Mora-Huertas, H. Fessi and A. Elaissari, *Adv. Colloid Interface Sci.*, 2011, **163**, 90-122.
51. G. Wypych, *Handbook of Solvents*, Toronto − New York, 2001.
52. Y. Liu, K. Kathan, W. Saad and R. K. Prud'homme, *Phys. Rev. Lett.*, 2007, **98**, 036102.
53. V. Kumar and R. K. Prud'homme, *Chem. Eng. Sci.*, 2009, **64**, 1358-1361.
54. C. Wu and J. McNeill, *Langmuir*, 2008, **24**, 5855-5861.

Schemes, Tables, and Figures Captions

Scheme 1: (A) Molecular structures of Coumarin 153 (C153) and Nile Red (NR).

Scheme 2: Illustration of the possible distribution of C153 (yellow spheres) and NR (red spheres) inside the PVK NPs for one-and two-doped systems.

Table 1. Values of orientational parameters (wobbling and lateral diffusion relaxation time constants, τ_R and τ_D, respectively; square order parameter, S^2; cone semi-angle, θ_0, wobbling and lateral diffusion coefficients, D_W and D_L, respectively) for PVK:C153 (0.22-2.72 wt%) and PVK:NR (0.63-1.60 wt%),

Table 2. Values of orientational parameters (wobbling and lateral diffusion relaxation time constants, τ_R and τ_D, respectively; square order parameter, S^2; cone semi-angle, θ_0, wobbling and lateral diffusion coefficients, D_W and D_L, respectively) for PVK:C153 (0-2.72 wt%):NR (1.60 wt%).

Table 3. Values of orientational parameters (wobbling and lateral diffusion relaxation time constants, τ_R and τ_D, respectively; square order parameter, S^2; cone semi-angle, θ_0, wobbling and lateral diffusion coefficients, D_W and D_L, respectively) for PVK:C153 (2.72 wt%):NR (0-1.60 wt%).

Figure 1. Representative emission anisotropy r(t) decays of water suspensions containing: (A) PVK:C153 (0.22 wt%, (1); 2.72 wt%, (2)) and (B) PVK:NR (0.63 wt%, (1); 1.60 wt%, (2)). The solid lines are from the best exponential fit. IRF is the instrumental response function. The excitation and emission wavelengths are indicated in the inset.

Figure 2. Representative emission anisotropy r(t) decays of water suspensions containing: (A) PVK:C153 (0.14 wt%, (1); 2.72 wt%, (2)):NR (1.60 wt%) and (B) PVK:C153 (2.72 wt%):NR (0.08, (1); 1.60 wt%, (2)). The solid lines are from the best exponential fit. IRF is the instrumental response function. The excitation and emission wavelengths are indicated in the inset.

Figure 3. (A) Variation of the wobbling (τ_R) and lateral diffusion (τ_D) relaxation time constants with the dye content for PVK:C153 (0.22-2.72 wt%). (B) Variation of the square order parameter (S^2) and cone semi-angle (θ_0) values with the dye content for PVK:C153 (0.22-2.72 wt%). The excitation and observation wavelengths were 410 and 510 nm, respectively.

Figure 4. (A) Variation of the wobbling (τ_R) and lateral diffusion (τ_D) relaxation time constants with the dye content for PVK:NR (0.63-1.60 wt%). (B) Variation of the square order parameter (S^2) and cone semi-angle (θ_0) values with the dye content for PVK:NR (0.63-1.60 wt%). The excitation and observation wavelengths were 510 and 610 nm, respectively.

Figure 5. (A) Variation of the wobbling (τ_R) and lateral diffusion (τ_D) relaxation time constants with the dye content for PVK:C153:NR (0.22-2.72 wt% C153; 1.60 wt% NR). (B) Variation of the square order parameter (S^2) and cone semi-angle (θ_0) values with the dye content for PVK:C153:NR (0-2.72 wt% C153; 1.60 wt% NR). The excitation and observation wavelengths were 510 and 610 nm, respectively.

Figure 6. (A) Variation of the wobbling (τ_R) and lateral diffusion (τ_D) relaxation time constants with the dye content for PVK:C153:NR (0-1.60 wt% NR; 2.7 wt% C153). (B) Variation of the square order parameter (S^2) and cone semi-angle (θ_0) values with the dye content for PVK:C153:NR (0-1.60 wt% NR; 2.7 wt% C153). The excitation and observation wavelengths were 410 and 510 nm, respectively.

Scheme 1

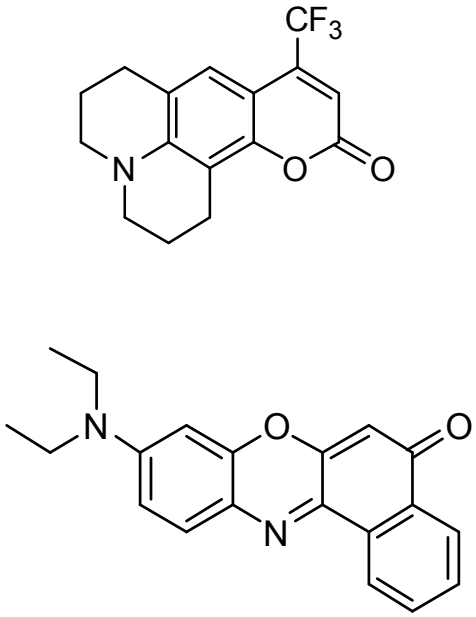

Scheme 2

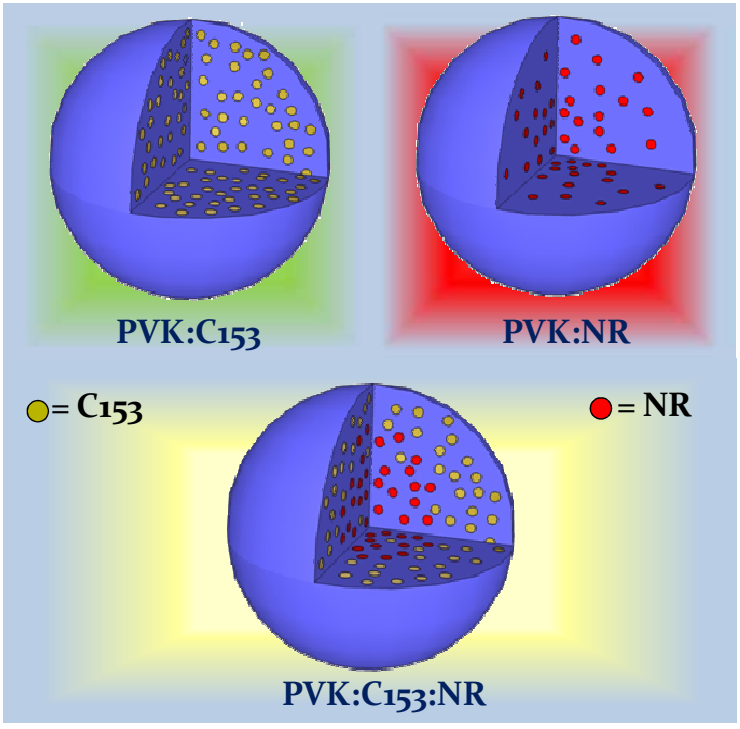

Table 1

	wt%	τ_R / ns	τ_D / ns	S^2	θ_0 / deg	$D_W \times 10^{-8}$ / s^{-1}	$D_L \times 10^8$ / m^2 s^{-1}
PVK:C153	0.22	0.20	4.63	0.62	32	4.17	3.24
	0.54	0.19	3.43	0.54	36	5.36	4.37
	1.08	0.18	2.42	0.47	39	6.34	6.20
	2.18	0.15	1.78	0.37	45	9.79	8.43
	2.72	0.14	1.57	0.33	47	11.12	9.55
PVK:NR	0.63	0.31	12.2	0.67	29	2.20	1.23
	0.95	0.32	8.01	0.61	32	2.54	1.87
	1.27	0.32	4.41	0.56	35	3.03	3.40
	1.60	0.30	3.09	0.52	37	3.56	4.85

Table 2

wt% C153	τ_R / ns	τ_D / ns	S^2 / a. u.	θ_0 / deg	$D_W \times 10^{-8}$ / s^{-1}	$D_L \times 10^8$ / m^2 s^{-1}
0	0.30	3.09	0.52	37	3.56	4.85
0.14	0.34	3.97	0.43	41	3.64	3.78
0.54	0.30	4.38	0.32	47	5.11	3.42
1.09	0.31	5.12	0.35	46	4.88	2.93
1.63	0.33	5.96	0.37	45	4.45	2.52
2.18	0.33	6.93	0.39	44	4.31	2.16
2.72	0.37	7.00	0.39	44	3.85	2.14

Table 3

wt% NR	τ_R / ns	τ_D / ns	S^2 / a. u.	θ_0 / deg	$D_W \times 10^{-8}$ / s^{-1}	$D_L \times 10^7$ / $m^2\ s^{-1}$
0	0.14	1.57	0.33	47	11.1	0.96
0.08	0.13	1.34	0.32	47	11.8	1.12
0.15	0.12	1.30	0.29	49	13.7	1.15
0.32	0.062	0.90	0.23	53	29.6	1.67
0.63	0.045	0.78	0.17	57	44.5	1.92
0.96	0.031	0.70	0.16	58	66.1	2.14
1.60	0.031	0.69	0.16	58	66.1	2.17

Figure 1

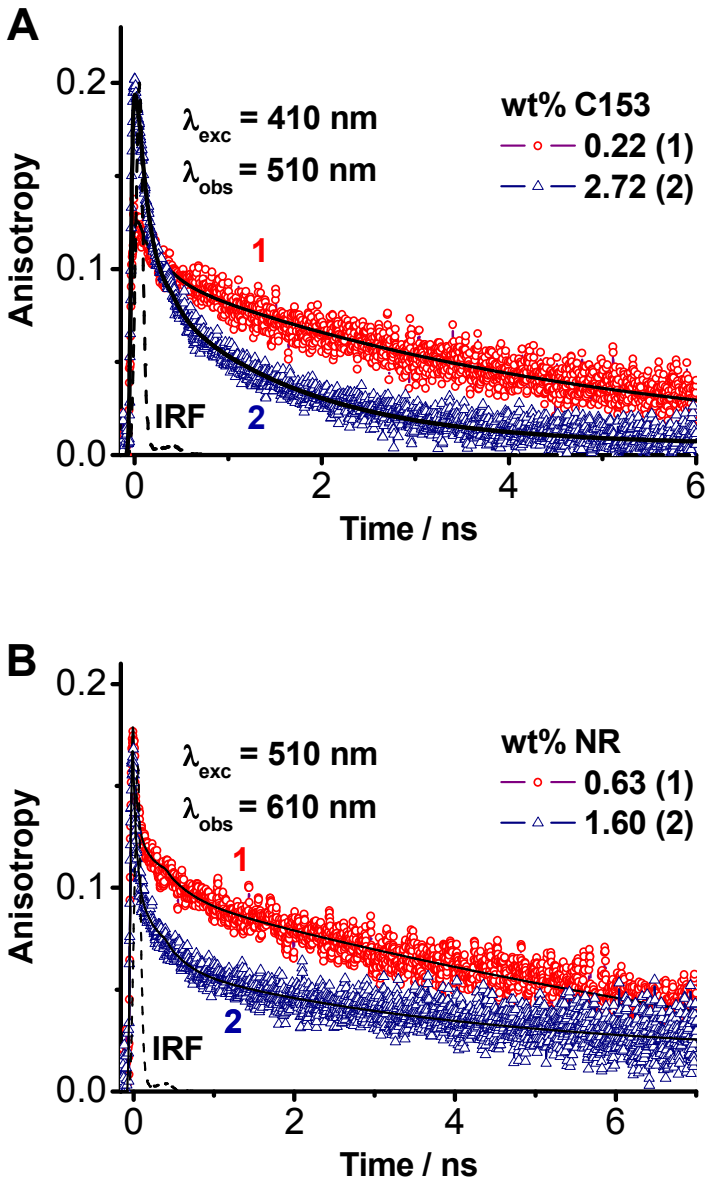

Figure 2

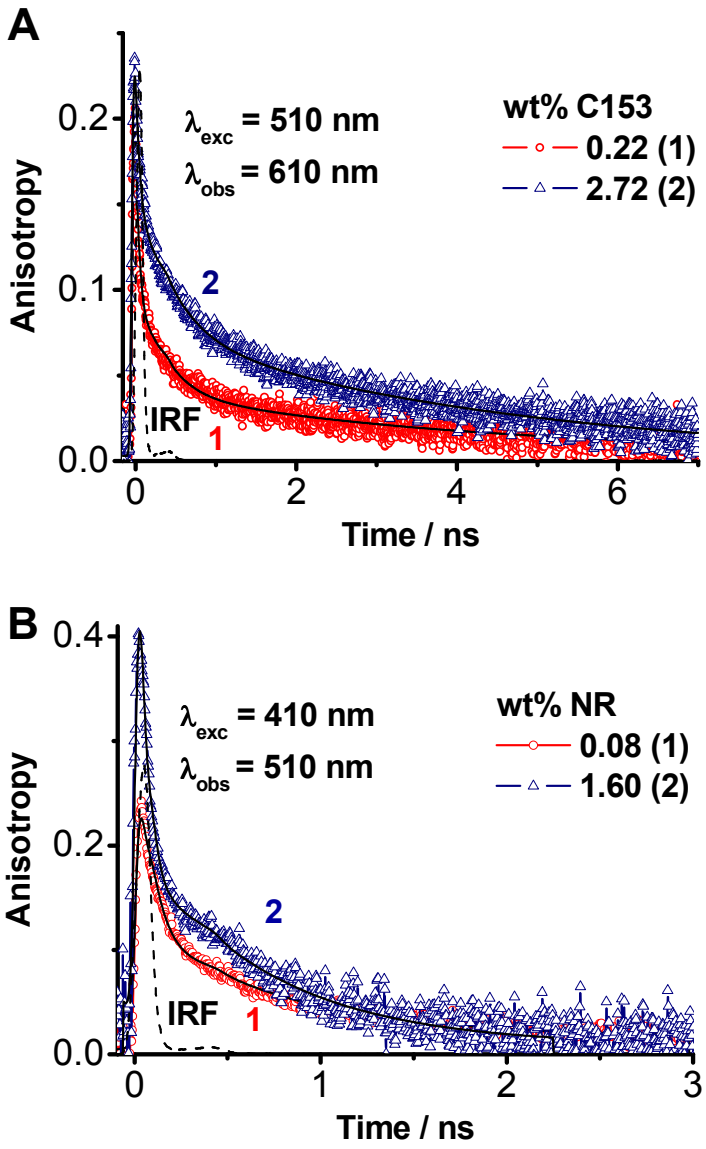

Figure 3

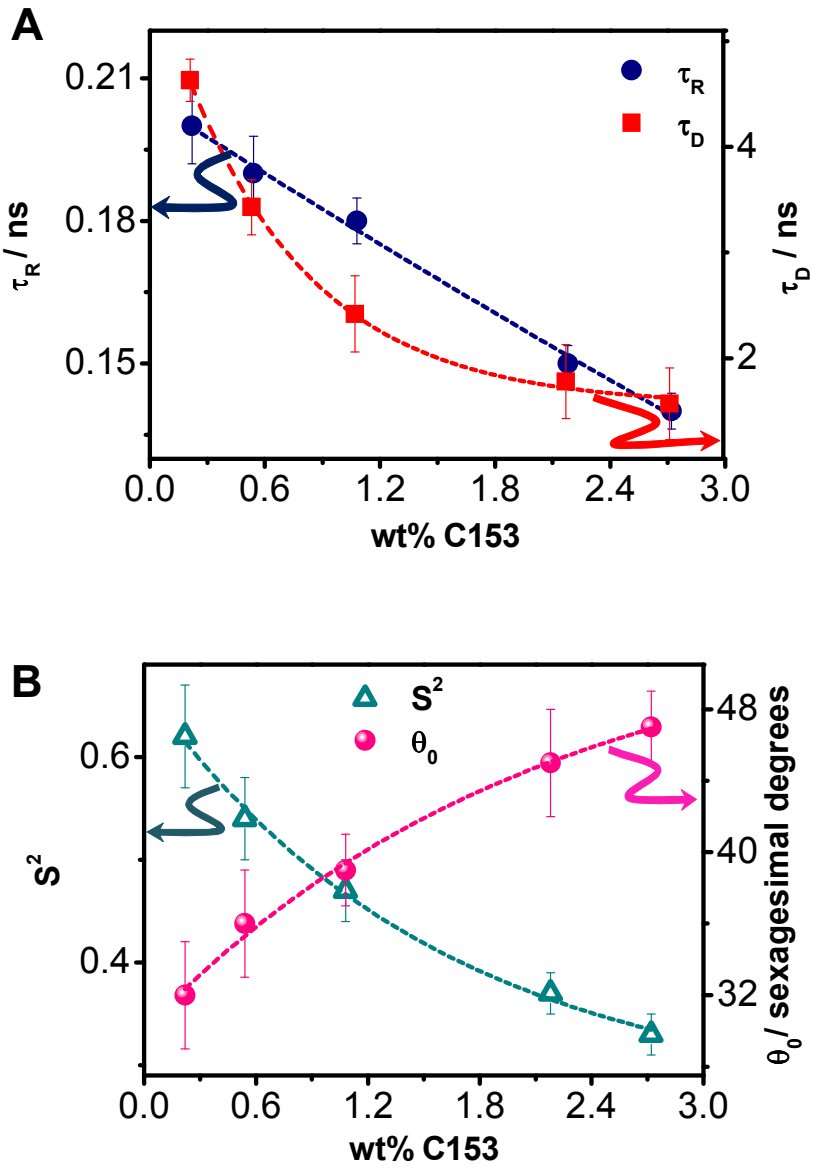

Figure 4

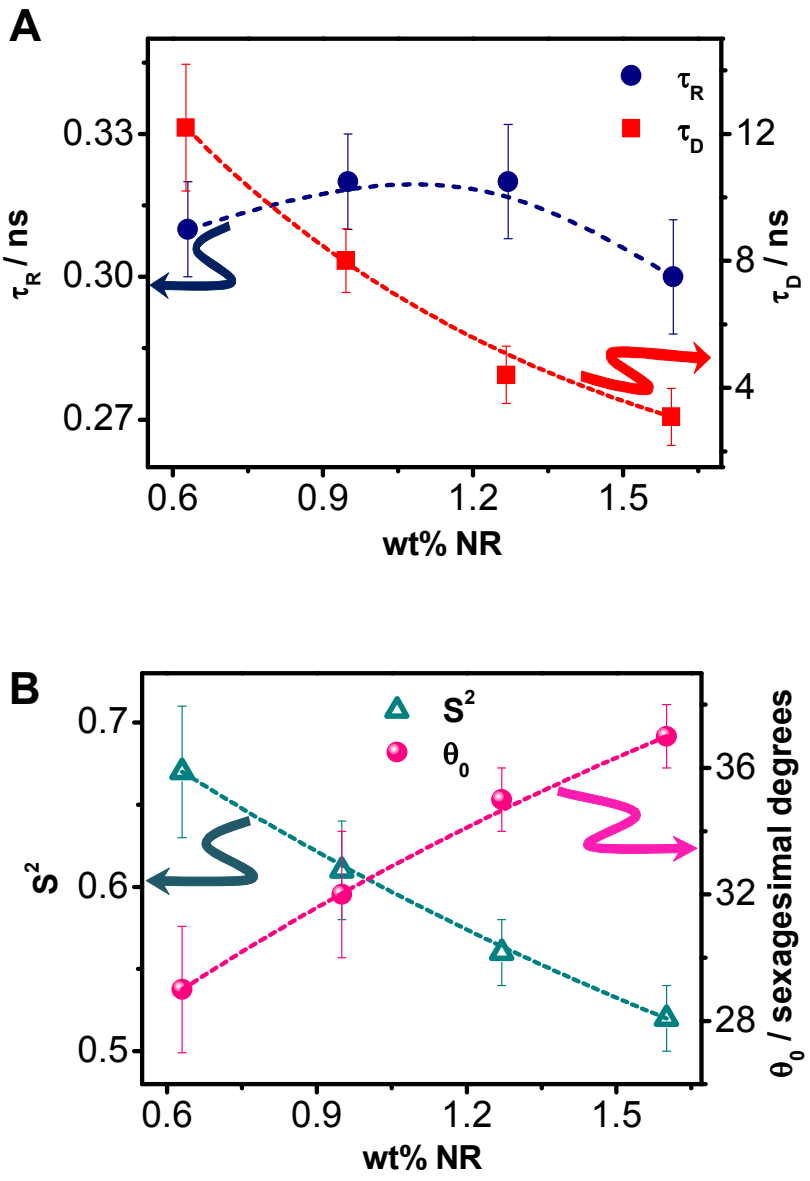

Figure 5

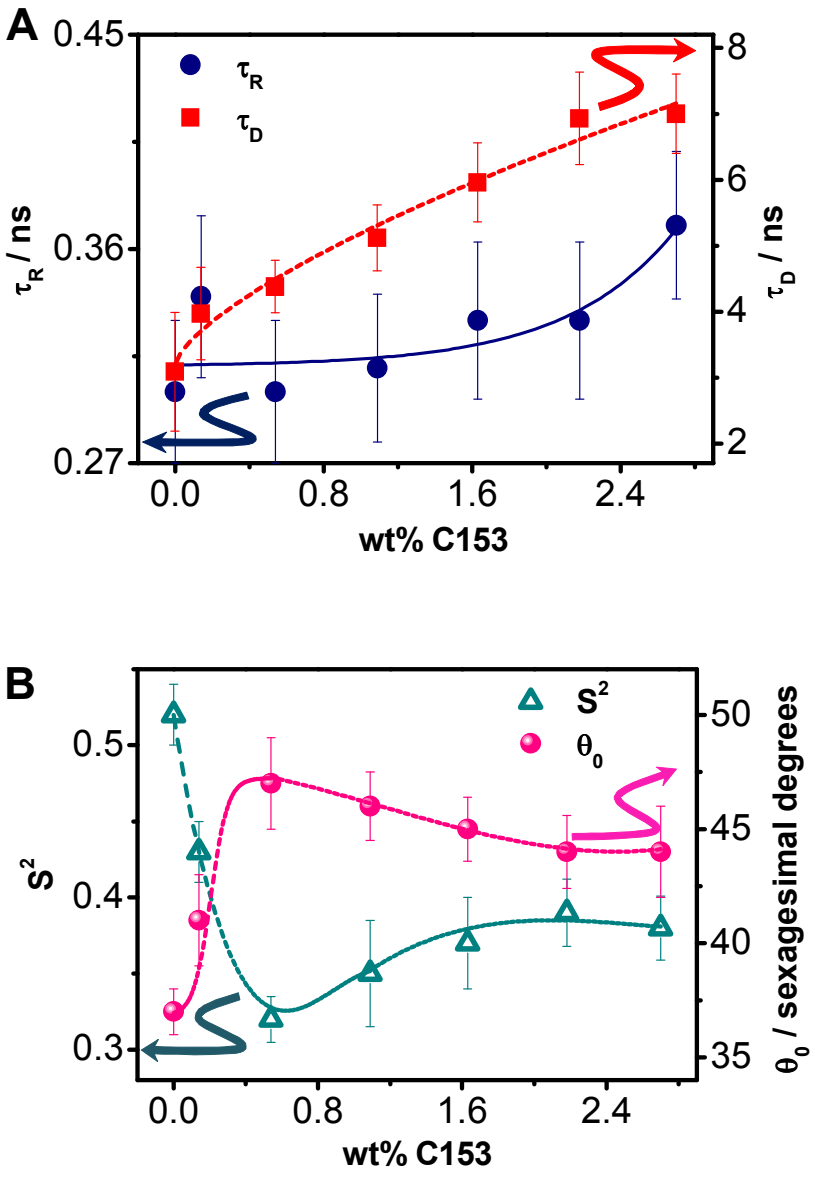

Figure 6

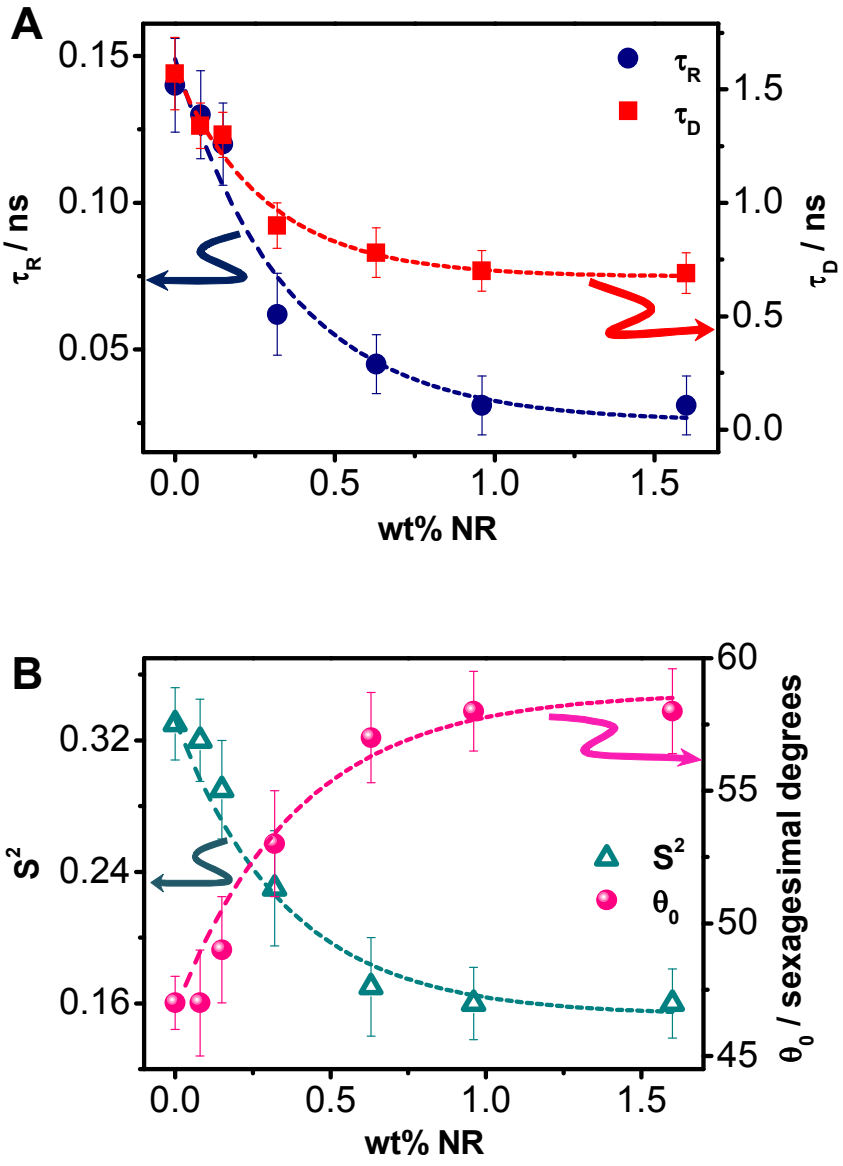

Table of Contents Graphic